Available online at www.sciencedirect.com

ScienceDirect

Proceedings of the Combustion Institute 37 (2019) 4137–4144

Proceedings of the Combustion Institute

www.elsevier.com/locate/proci

Measuring heat flux to a porous burner in microgravity

Akshit Markan, Peter B. Sunderland, James G. Quintiere*, John L. de Ris, Howard R. Baum

Department of Fire Protection Engineering, University of Maryland, College Park, MD USA

Received 1 December 2017; accepted 24 May 2018
Available online 27 June 2018

Abstract

Flame heat flux absorbed by a porous gas-fueled burner is measured in microgravity. The burner's perforated copper plate serves as a slug calorimeter in which two heat flux thermopile sensors are embedded. The slug calorimeter provides the average heat flux over the burner surface as a function of time. The 25 mm diameter burner is calibrated as a slug calorimeter in normal gravity using a known radiative heat flux with step changes. Microgravity diffusion flames were observed in NASA Glenn's 5.18-s Zero Gravity Research Facility, and average heat fluxes measured with the calorimeter agree with the locally measured heat fluxes through a theoretical distribution function. The results show that the average slug calorimeter heat flux and the two local heat flux measurements are in harmony over a wide range of microgravity flame fluxes ranging from 5–20 kW/m^2, with the edge heat flux much higher. Transient and nearly steady results are presented.

Keywords: Calorimeter; Fire safety; Diffusion flames; Laminar flames; Spacecraft

1. Introduction

Measurements of transient heat flux to solid surfaces have been reviewed comprehensively [1,2]. The preferred methods in fire research involve temperature-gradient (differential) measurement gauges [3–7] and calorimetric or energy balance methods [8–17] because these are suitable for high heat fluxes and temperatures. Commonly used gradient-based devices include Gordon gauges [3] and Schmidt–Boelter (SB) gauges [6]. These gauges, which have a good heat sink, must be carefully calibrated [7]. When the SB-thermopile gauges are used to measure heat flux absorbed by a porous burner, a special calibration technique was developed [8].

Slug calorimeters allow the measurement of incident heat flux based on the temperature of an isothermal slug, typically made of copper. Slug calorimeters are simple to design, and they have been standardized [9]. NASA has utilized flat-faced slug calorimeters for use on spacecraft during re-entry into the atmosphere [10]. Thin-skin calorimeters have been developed for measuring the irradiation for large-scale compartment fire testing [11,12]. Recently, Hubble [13] developed a directional slug calorimeter for mea-

* Corresponding author.
E-mail address: jimq@umd.edu (J.G. Quintiere).

https://doi.org/10.1016/j.proci.2018.05.006
1540-7489

Nomenclature

A	surface area
B	Spalding B number
c	specific heat
D	diameter
e	thermal effusivity
F	heat flux to semi-infinite back
h	convective heat transfer coefficient
h_o	effective heat transfer coefficient between semi-infinite back and plate
h_{rod}	effective heat transfer coefficient between sensor rod and plate
H	thickness of copper plate
k	thermal conductivity
$\dot{m}''$	fuel mass flux
$\dot{m}$	mass flow rate
$(mc)_{Cu}$	heat capacity of copper
p	pressure
$\dot{q}''$	heat flux
$\dot{Q}$	heat loss
r	radius
R	burner radius
R^*	radius of heat flux sensor
t	time
T	temperature
x	depth along the semi-infinite back
X	mole fraction
Greek	
ξ	ellipsoidal coordinate
η	ellipsoidal coordinate
α	absorptivity
δ	thermal length
ϵ	emissivity or ellipsoidal aspect ratio
ρ	density
σ	Stefan–Boltzmann constant
Subscripts	
abs	absorbed
avg	average
b	semi-infinite back
Cu	copper plate surface excluding holes
$Cu + holes$	copper plate surface including holes
g	fuel gas
h	hole
i	incident
o	semi-infinite back at $x = 0$
rod	sensor rod
∞	ambient

suring heat flux in a severe high temperature environment.

The burner considered here has been developed for the ACME Burning Rate Emulation (BRE) flight experiment [8,14,15]. It is a 25 mm diameter porous gas-fueled burner that emulates the burning of condensed phase fuels. The burner has a flat copper surface that is equipped with two Schmidt–Boelter type heat flux sensors for local measurements [8,14,15]. The BRE flames have been shown to emulate liquid and solid pool fires. For liquid pool fires, the heat flux and burning rate vary significantly in the radial direction [16,17]. Hence, a slug calorimeter is ideal for measuring the average heat flux from the flame. Tests are performed in microgravity with an eye toward spacecraft fire safety.

The objective of the current study is to measure the local and average absorbed heat flux on the BRE burner in microgravity. An analytical model is presented to relate the local and average heat fluxes. It will be shown that the accuracy of the heat flux measurements, both local and average, are brought into good agreement by the theory.

2. Model

The BRE burner consists of a copper plate perforated with holes, a ceramic flow straightener and stainless-steel sidewalls. The exposed surface of the copper plate is coated with a paint of measured absorptivity and emissivity [18]. The burner has two SB non-water-cooled heat flux sensors and two K-type thermocouples in the burner surface for measuring the local absorbed heat flux and the slug temperature, respectively. The locations of the thermocouples and heat flux sensors are at the center and a radius of $R^* = 8.25$ mm.

The slug calorimetric model provides a direct measurement of the average absorbed heat flux for the BRE burner by utilizing only the temperature measurements of the copper plate. Here, the 25 mm burner with a copper slug thickness of 6.35 mm is used. A schematic of the top copper plate of the burner encased by a control volume is shown in Fig. 1. This copper slug is exposed to an incident heat flux $\dot{q}_i''$ and it loses heat through re-radiation, convection (during calibration), heat transfer to the flowing gas in the holes, heat transfer to the two sensor rods, and heat transfer to the sidewalls and flow straightener. Figure 1 shows two heating conditions: (1) uniform radiant heat flux for calibration, and (2) heat from the flame in the microgravity drop tests. Both are important to understand the calibration and the flame measurements.

2.1. Description of the calorimeter model

It is justified that the temperature of the copper slug does not vary spatially since its thermal response time, based on a copper thermal diffusivity of 10^{-4} m^2/s, is less than 0.5 s with respect to the copper depth of 6.35 mm and diameter of 25 mm. The sidewalls and the flow straightener are modeled as a single homogeneous semi-infinite body. The heat transfer between the copper plate and this semi-infinite body is modeled as a linear heat flow ($h_o(T - T_o)$) through the air gap. The fuel enters the

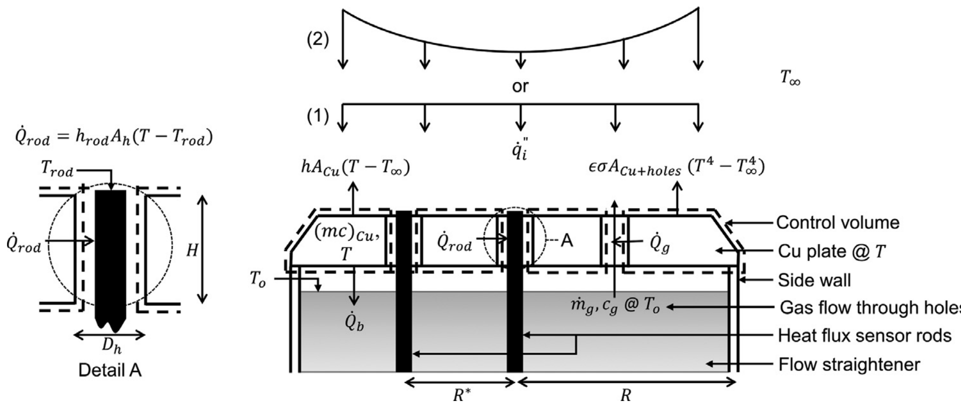

Fig. 1. Schematic representation (not drawn to scale) of the top copper plate of the BRE burner.

porous copper plate at the temperature of the back (straightener + sidewalls) T_o and is assumed to attain the temperature of the copper plate T before exiting the plate. The re-radiation from the top surface of the copper plate and the holes is to the ambient. The re-radiation area is the entire control volume surface area over the top of the copper plate, including the projection of the holes, $A_{Cu+holes}$. The convective heat loss is from the exposed top surface of the solid copper, A_{Cu}. This term is only present during calibration and not relevant for the microgravity flame measurements.

2.2. *Energy conservation for the copper calorimeter during calibration*

As shown in Fig. 1, the porous copper plate is modeled as a lumped system (uniform temperature) where the net heat absorbed by the copper plate is represented by several different energy components. Each term will be described as the model is developed. The following conservation equation for the copper is written with application first to the uniform radiant flux case in calibration:

$$\dot{q}''_{abs} A_{Cu+holes} = \alpha\, \dot{q}''_i\, A_{Cu+holes} = (mc)_{Cu}\,(dT/\,dt) + \epsilon\,\sigma A_{Cu+holes}\left(T^4 - T_\infty^4\right) + h\,A_{Cu}(T - T_\infty) + \dot{Q}_g + \dot{Q}_{rod} + \dot{Q}_b. \quad (1)$$

Here, $(mc)_{Cu}$ is the heat capacity of copper, α is the absorptivity of the top surface, ϵ is the emissivity and h is the convective heat transfer coefficient. Each term in Eq. (1) is further described below.

The rate of change of internal energy of the copper plate is $(mc)_{Cu}\,(dT\,/\,dt)$. The temporally-resolved temperature of the copper plate is measured and $dT\,/\,dt$ is determined from the measured temperatures using the built-in 19-point LINEST function in MS Excel.

The control volume in Fig. 1 shows that heat is lost from the copper plate to the gas flowing through the holes at a mass flow rate of $\dot{m}_g$. The gas temperature increases from T_o entering to T at the exit of the copper slug. The heat loss to the fuel gas $\dot{Q}_g$ can be expressed as

$$\dot{Q}_g = \dot{m}_g\, c_g\,(T - T_o), \quad (2)$$

where c_g is the specific heat of the gas mixture. The mass flow rate of the fuel and the copper temperature are measured. The temperature of the gas at entry, i.e., the temperature of the semi-infinite back, is derived below.

The re-radiation term, $\epsilon\,\sigma\,A_{Cu+holes}\,(T^4 - T_\infty^4)$, requires knowledge of the emissivity. The emissivity of the top surface corresponds to paint used (Nextel Suede 3101), which has been measured as approximately 1 [18].

The convective loss term, $h\,A_{Cu}\,(T - T_\infty)$, requires the heat transfer coefficient. During calibration, the burner surface is in the vertical plane. Thus, the convective heat transfer coefficient is determined assuming natural convection from a vertical plane [19]. h as given in Ref. [19] is a function of temperature and diameter of the burner, lying in the range of 10–30 W/m^2-K for the current calibration tests.

Detail A in Fig. 1 indicates that the copper plate transfers heat to the heat flux sensor rods. This depends on the level of contact between the rods and the plate. An effective heat transfer coefficient, h_{rod}, is assumed. Thus, the heat loss to the sensor rods is

$$\dot{Q}_{rod} = h_{rod}\,A_h\,(T - T_{rod}), \quad (3)$$

where $A_h\,(=\pi D_h H)$ is the surface area of the hole and T_{rod} is the temperature of the thermopile. The parameter h_{rod} is a calibration parameter determined for the burner.

The heat transfer from the back of the copper plate is considered as a linear heat flow to the semi-infinite medium (sidewalls + flow straightener) and it is expressed as

$$\dot{Q}_b = h_o\,A_{Cu+holes}\,(T - T_o), \quad (4)$$

where h_o is an effective heat transfer coefficient for the space between the copper and the semi-infinite back. The parameter h_o needs to be determined in the calibration, and temperature T_o is derived below.

The material behind the copper plate consists of stainless steel sidewalls and a ceramic flow straightener. The heat transfer from the copper plate is imposed on this semi-infinite body from Eq. (4) and the heat flux is designated as

$$F = h_o\,(T - T_o). \tag{5}$$

An approximate integral solution for a semi-infinite solid, with an imposed time varying surface heat flux (F) is now obtained. The temperature at any point along the semi-infinite back is defined as $T_b(x, t)$ such that $T_b(0, t) = T_o$. The back (steel walls and ceramic) has a specific heat c_b, density ρ_b and thermal conductivity k_b, which are constant for a specific burner configuration. The heat conduction equation for the semi-infinite back is

$$\rho_b c_b(\partial T_b/\partial t) = k_b\left(\partial^2 T_b/\partial x^2\right). \tag{6}$$

For the integral model, the back temperature T_b is assumed to be

$$T_b = a + b(x/\delta) + c(x/\delta)^2, \tag{7}$$

where a, b, and c are constants and δ is the thermal length, i.e., the penetration depth of the thermal layer. The boundary conditions for the back temperature are defined such that the heat flux at the bottom surface of the copper plate ($x = 0$) is $-k_b\ \partial T_b/\partial x = F$, and at infinity ($x = \delta$), the temperature is ambient. Using the boundary conditions and Eq. (7) for the back temperature T_b, we can find the constants a, b, and c. This yields

$$T_b = T_\infty + \frac{\delta F}{2k_b}\left(1 - \frac{x}{\delta}\right)^2. \tag{8}$$

A solution for δ is obtained by integrating Eq. (6) from 0 to δ. Inserting Eq. (8) yields the thermal length,

$$\delta = \left[\frac{6k_b \int_0^t F\,dt}{\rho_b c_b F}\right]^{1/2}. \tag{9}$$

This allows T_o to be expressed as

$$T_0 = T_\infty + \frac{h_o}{e_b}\left[1.5\,(T - T_0)\int_0^t (T - T_0)\,dt\right]^{1/2}, \tag{10}$$

where $e_b = (k_b\rho_b c_b)^{1/2}$ is the thermal effusivity of the semi-infinite back. The parameters e_b and h_o are burner-specific and need to be determined. The explicit finite difference scheme can be utilized to solve Eq. (10). The heat loss to the back can then be found.

2.3. Determination of burner-specific parameters

The three parameters h_{rod}, h_o and e_b are burner-specific and must be determined through calibration. Three conditions are required. Two conditions are given for the absorbed radiant heat flux measured at the beginning and the end of the calibration. This heat flux is found using a Medtherm heat flux sensor traceable to a NIST standard [18]. Substituting the measured absorbed heat flux $\dot{q}''_{abs}$ into Eq. (1) at $t = 0$ and $t = 5$s, yields two of the parameters h_{rod} and h_o. The third parameter e_b comes from Eq. (10) that relates h_o and e_b. The procedure utilized to determine the burner-specific quantities is discussed below.

3. Calibration of the BRE burner as a slug calorimeter

A radiant infrared heat source is utilized in normal gravity to calibrate the 25 mm diameter BRE burner heat flux instruments. The absorbed heat flux from the radiant source is measured using the Medtherm SB-heat flux sensors in the burner. These are 0.8 mm diameter uncooled heat flux sensors located at the center and a radius of $R^* = 8.25$ mm. The paint used on the sensors and the copper surface is Nextel Suede 3101 that has been found to have an emissivity of 1 and an absorptivity of 0.98 [18]. The Medtherm heat flux sensors have been calibrated against a NIST standard as illustrated in Ref. [18]. The calibration setup, shown in Fig. 2, consists of the burner mounted on a stand with its top surface vertical and facing the radiant heater. During the calibration there is no gas flow through the burner; hence, $\dot{Q}_g = 0$. The variation of heat flux over the face of the burner was found to be negligible.

Adjusting the distance between the burner and the heater changes the heat flux at the burner surface. The calibration began with a heat flux of about 5 kW/m^2. This was increased in discrete steps to about 10 kW/m^2 and then decreased in discrete steps to zero. The heat flux is maintained at each level for about 2 minutes. The local heat flux sensors record the absorbed radiant heat flux by the thermopile. The ambient temperature, the copper temperature and the sensor temperatures are recorded at every time step. The initial and final SB heat flux sensor readings are used to calibrate the copper slug calorimeter and to determine the quantities: h_{rod}, h_o and e_b.

It was found for the 25 mm BRE burner: $h_{rod} = 1408$ W/m^2-K, $h_o = 81$ W/m^2-K, $e_b = 4899$ (W/m^2-K)-s$^{1/2}$. The calorimetry model, given by Eq. (1), can now be used to determine the average absorbed heat flux using these quantities. The other

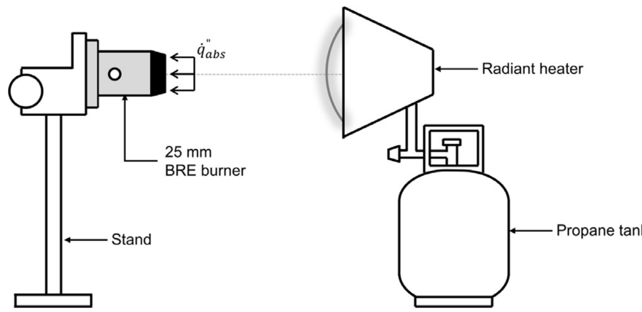

Fig. 2. Setup for calibration of the BRE as a calorimeter.

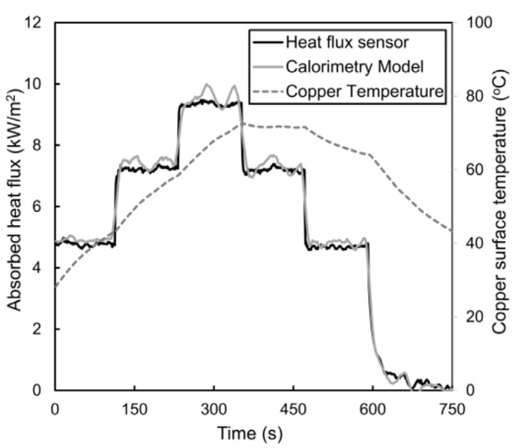

Fig. 3. Verification of the calorimetry model for the BRE burner.

fixed parameters for the 25 mm BRE burner are: $A_{Cu} = 3.448 \times 10^{-4}$ m^2, $A_{Cu+holes} = 4.91 \times 10^{-4}$ m^2, $A_h = 3.55 \times 10^{-5}$ m^2, and $(mc)_{Cu} = 7$ J/K.

To demonstrate its accuracy and response, the calorimeter absorbed heat flux is compared to the NIST calibrated heat flux sensor over step changes as shown in Fig. 3. The calorimetry model determines the absorbed heat flux accurately over these sharp changes in time. The copper temperature utilized for the calorimeter heat flux is also plotted in Fig. 3.

4. Measurement of absorbed heat flux in microgravity

Two different heat flux measurement techniques are used to determine the absorbed flame total convective and radiative heat flux for the 25 mm BRE burner during microgravity tests at NASA Glenn's 5.18-s Zero Gravity Research Facility [15]: (a) local measurement using SB-Medtherm thermopile heat flux sensors and (b) the average measurement using slug calorimetry model given by Eq. (1). The SB-sensors are corrected for temperatures differently from the copper surface as explained in Ref. [8]. These sensors are located at the center and a radius of $R^* = 8.25$ mm.

The same BRE burner-specific parameters are used to determine the average flame heat flux over the burner surface during each microgravity test. For this Eq. (1) is reformulated to apply to the case of flame heating as

$$\dot{q}''_{abs} A_{Cu+holes} = (m\,c)_{Cu}\,(dT\,/\,dt) + \epsilon\,\sigma\,A_{Cu+holes}\left(T^4 - T_\infty^4\right) + \dot{Q}_g + \dot{Q}_{rod} + \dot{Q}_b. \tag{11}$$

Here $\dot{Q}_g$ is required, while the convective heating term is not relevant. Figure 4 shows the average absorbed heat flux measured by the calorimeter along with the local heat flux sensor measurements for two representative microgravity test durations of about 5 s. Negative times correspond to heat fluxes in normal gravity during the ignition process before microgravity. The average heat flux in normal gravity is 44–48 kW/m^2, but at the end of the 5-s in microgravity, approaching a quasi-steady state, this reduces to 12–17 kW/m^2. The flow effects of buoyancy in 1 g causes the flame to be much closer to the surface that causes the average heat flux to be much higher in 1 g than in microgravity. The two local sensor heat fluxes are lower, as discussed below.

The highest heat flux is at the edge, where the flame is closest to the burner. Indeed, this can be deduced from the pure conduction problem [20]. More thoroughly this is shown in Ref. [21], where the pure diffusive combustion problem is formulated in oblate ellipsoidal coordinates (ξ, η) and shown to be one-dimensional depending only on the ellipsoidal coordinate (ξ) and time. The diffusive heat flux in microgravity is proportional to the temperature gradient ($\dot{q}''(r) = -k\nabla T$). The BRE burner geometry is approximated in this solution as an axially symmetric porous disc (with ellipsoidal aspect ratio $\epsilon = 0$). The mathematical representation of the gradient operator from ellipsoidal to cylindrical coordinates gives the surface heat flux

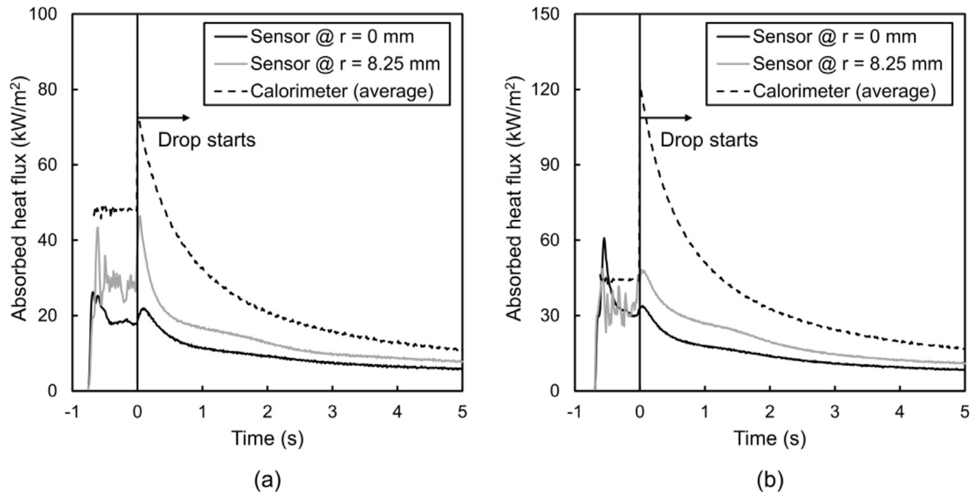

Fig. 4. Heat flux for 25 mm burner tests with conditions: (a) C_2H_4 as fuel, $X_{O_2} = 0.21$, $p = 1.0$ atm, $\dot{m}'' = 3.61$ g/m^2-s, (b) C_2H_4 as fuel, $X_{O_2} = 0.30$, $p = 0.7$ atm, $\dot{m}'' = 3.20$ g/m^2-s.

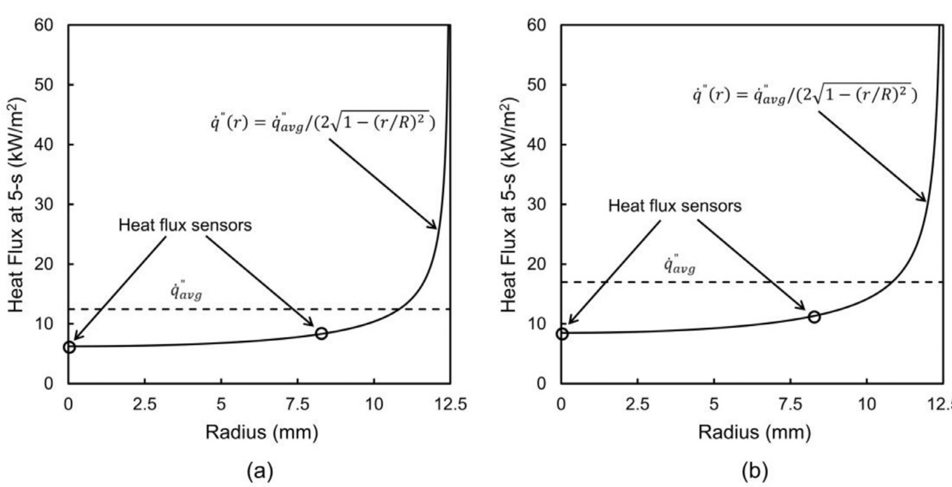

Fig. 5. Radial distribution of heat flux after 5-s for 25 mm burner tests with conditions: (a) C_2H_4 as fuel, $X_{O_2} = 0.21$, $p = 1.0$ atm, $\dot{m}'' = 3.61$ g/m^2-s, (b) C_2H_4 as fuel, $X_{O_2} = 0.30$, $p = 0.7$ atm, $\dot{m}'' = 3.20$ g/m^2-s.

as:

$$\dot{q}''(r) = -k\,[\nabla T]_{\xi=0} = \frac{1}{\sqrt{1-(r/R)^2}}\left[-\frac{k}{R}\frac{dT}{d\xi}\right]_{\xi=0} = \frac{\dot{q}''(r=0)}{\sqrt{1-(r/R)^2}}. \qquad (12)$$

The average heat flux is determined as $\dot{q}''_{avg} = \int_0^R \dot{q}''(r)\,2\pi r\,dr/\pi R^2$, and hence, the surface heat flux distribution can be expressed in terms of the average as

$$\dot{q}''(r) = \frac{\dot{q}''_{avg}}{2\sqrt{1-(r/R)^2}}. \qquad (13)$$

This equation relates the local measurements to the average calorimeter heat flux measurement. According to the theoretical Eq. (13), heat flux reaches a singularity at the edge for the flat disc solution. However, realistically the flame is close to the edge and hence, the heat flux is very high (not infinite for nonzero ϵ).

Let us test Eq. (13) with the heat flux measurements in the nearly steady regime at the end of the 5 s duration, for the tests of Fig. 4. The radial

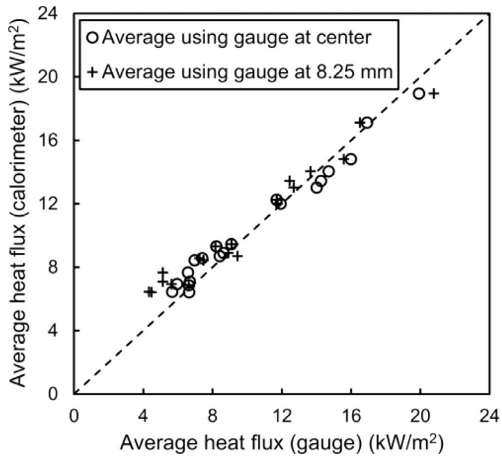

Fig. 6. Calorimeter average heat flux vs. average heat flux derived from gauge measurement at center and $R^* = 8.25$ mm after 5-s for 25 mm microgravity tests.

distribution of heat flux using Eq. (13) based on the copper slug calorimeter measurement ($\dot{q}''_{avg}$) is in remarkable agreement with the two local SB-heat flux measurements as shown in Fig. 5. The distribution computed from the theory by the slug calorimeter average heat flux measurement nearly identically matches the two local processed thermopile measurements.

The model is further applied to 18 microgravity tests conducted using the 25 mm BRE burner [15]. The calorimeter average heat flux at 5 s is plotted in Fig. 6 for each microgravity test with the average heat flux derived from each sensor measurement using Eq. (13). These are nearly steady heat flux results, although the flame is still growing. Figure 6 contains the entirety of the 18 microgravity tests and demonstrates the overall consistency of the calorimeter average heat flux with the theoretical average using Eq. (13) based on the local heat flux sensor measurements. The consistency is mostly within +/− 10 % except at low heat flux.

The average flame heat flux for the 25 mm emulated burning in microgravity varies between 5–20 kW/m^2 and represents a wide range of condensed fuels. This heat flux is directly related to condensed fuel's B number [14,15].

Conclusions

An absorbed heat flux measurement technique for the BRE burner flames in microgravity is presented. This is based on slug calorimetry and thermopile sensors. The local heat flux is measured using burner embedded heat flux sensors and the average heat flux is measured using the burner top copper plate as a calorimeter. The calibration of the calorimeter with a known radiant heat flux displays good accuracy and time response to allow its use in microgravity. The local heat flux measurements in microgravity have an inverse-square root dependence on radius, with the highest fluxes at the edge. The heat flux from a 25 mm disc burning in microgravity is expected to be about 5–20 kW/m^2 depending on the emulated fuel. The calorimeter technique is planned for use in proposed ACME-ISS experiments where steady conditions will be sought.

Acknowledgments

This research was funded by NASA's International Space Station Research Program (grant number NNX15AD06A), with D.P. Stocker serving as contract monitor.

References

[1] T.E. Diller, Advances in Heat Flux Measurement, in Advances in Heat Transfer, Academic Press, Boston, 1993, pp. 279–368.
[2] P.R.N. Childs, J.R. Greenwood, C.A. Long, *Proc. Inst. Mech. Eng. Part C* 213 (1999) 655–677.
[3] R. Gardon, *J. Heat Transfer* 82 (1960) 396–398.
[4] J.M. Hager, L.W. Langley, S. Onishi, T.E. Diller, *J. Thermophys. Heat Transfer* 7 (1992) 531–534.
[5] J.C. Godefroy, M. Clery, C. Gageant, D. Francois, Y. Servouze, *Thin Solid Films* 193 (1990) 924–934.
[6] C.T. Kidd, C.G. Nelson, in: Proceedings of the 41st International Instrumentation Symposium, 1975, pp. 347–368.
[7] W.M. Pitts, A.V. Murthy, J.L. de Ris, J.R. Filtz, K. Nygård, D. Smith, I. Wetterlund, *Fire Saf. J.* 41 (2006) 459–475.
[8] Y. Zhang, M. Kim, H. Guo, P.B. Sunderland, J.G. Quintiere, J.L. de Ris, D.P. Stocker, *Combust. Flame* 162 (2015) 3449–3455.
[9] ASTM E457-08 Standard Test Method for Measuring Heat-Transfer Rate Using a Thermal Capacitance (Slug) Calorimeter, ASTM International, West Conshohocken, PA, 2015.
[10] A. Nawaz, J.A. Santos, in: Proceedings of the 10th AIAA/ASME Joint Thermophysics and Heat Transfer Conference, 2010.
[11] J.P. Hidalgo, C. Maluk, A. Cowlard, C. Abecassis-Empis, M. Krajcovic, J.L. Torero, *Int. J. Thermal Sci.* 112 (2017) 383–394.
[12] P.S. Veloo, J.G. Quintiere, *J. Fire Sci.* 31 (2013) 410–423.
[13] D.O. Hubble, Directional Slug Calorimeter for Heat Flux Measurements, US Patent Application Publication No. 2015/0346042, 2015.
[14] Y. Zhang, M. Kim, P.B. Sunderland, J.G. Quintiere, J.L. de Ris, *Exp. Therm. Fluid Sci.* 73 (2016) 87–93.
[15] A. Markan, P.B. Sunderland, J.G. Quintiere, J.L. de Ris, D.P. Stocker, H.R. Baum, *Combust. Flame* 192 (2018) 272–282.
[16] K. Akita, T. Yumoto, *Proc. Combust. Inst.* 10 (1965) 943–948.
[17] A. Hamins, M. Klassen, J. Gore, S. Fischer, T. Kashiwagi, *Combust. Sci. Technol.* 97 (1994) 37–62.

[18] H. Kim, *Procedures to Obtain Accurate Measurement from a Gas Fueled Burner* Master's thesis, University of Maryland, College Park, 2014.
[19] C.O. Bennett, J.E. Myers, Momentum, Heat and Mass Transfer, McGraw-Hill, New York, 1962, p. 697.
[20] H.S. Carslaw, J.C. Jaeger, *Conduction of Heat in Solids*, 2nd ed, Oxford University Press, London, 1959.
[21] H.R. Baum, A. Atreya, *Fire Safety Sci.* 11 (2014) 1353–1367.